

Beckman Defense

A V Subramanyam

IITD

subramanyam@iitd.ac.in

Abstract

Optimal transport (OT) based distributional robust optimisation (DRO) has received some traction in the recent past. However, it is at a nascent stage but has a sound potential in robustifying the deep learning models. Interestingly, OT barycenters demonstrate a good robustness against adversarial attacks. Owing to the computationally expensive nature of OT barycenters, they have not been investigated under DRO framework. In this work, we propose a new barycenter, namely Beckman barycenter, which can be computed efficiently and used for training the network to defend against adversarial attacks in conjunction with adversarial training. We propose a novel formulation of Beckman barycenter and analytically obtain the barycenter using the marginals of the input image. We show that the Beckman barycenter can be used to train adversarially trained networks to improve the robustness. Our training is extremely efficient as it requires only a single epoch of training. Elaborate experiments on CIFAR-10, CIFAR-100 and Tiny ImageNet demonstrate that training an adversarially robust network with Beckman barycenter can significantly increase the performance. Under auto attack, we get a maximum boost of 10% in CIFAR-10, 8.34% in CIFAR-100 and 11.51% in Tiny ImageNet. Our code is available at <https://github.com/Visual-Conception-Group/test-barycentric-defense>.

1 Introduction

Optimal mass transport (OT), originally proposed by Monge in his seminal work [Monge, 1781], has gathered a widespread interest in the field of learning representations. The original deterministic OT problem was later relaxed by Kantorovich [Kantorovich, 1942] and considered a probabilistic transport problem. This formulation seeks solution for the optimal transport plan which can transport mass between two measures by incurring the minimum cost and is solved using a linear program. The modern day OT is also attributed to the phenomenal work of Kantorovich. Following the OT theory, barycenters in Wasserstein space was proposed

by Agueh and Carlier in their remarkable work [Agueh and Carlier, 2011]. Further, using entropic regularization [Cuturi, 2013], a fast method of computing barycenters was proposed by Cuturi and Doucet [Cuturi and Doucet, 2014]. Recent works address the challenge of computational complexity of barycenters using neural networks [Lacombe *et al.*, 2021]. In this work, we investigate the barycenters towards robust learning of deep learning models.

Deep learning systems have shown impressive performance in various applications. However, these systems are vulnerable to adversarial perturbations [Wong *et al.*, 2020], [Croce and Hein, 2020], [Xie *et al.*, 2019]. In order to counter these attacks, several defense mechanisms have also been proposed. In one of the early works, Szegedy *et al.* [Szegedy *et al.*, 2013] formulated the adversarial attack as an optimization problem and obtained the adversarial sample using L-BFGS. Several adversarial attacks have been proposed since Szegedy’s work [Goodfellow *et al.*, 2014; Kurakin *et al.*, 2016]. On the other hand, strong defense measures have been studied in [Madry *et al.*, 2017], [Theagarajan *et al.*, 2019], [Wong *et al.*, 2020], [Rebuffi *et al.*, 2021].

In the field of adversarial attacks and defense, l_p space has been extensively studied. However, only a few works investigate attacks under OT framework [Wong *et al.*, 2019], [Li *et al.*, 2021]. There are even fewer works which investigate robustness using OT theory [Kwon *et al.*, 2020], [Subramanyam and Raj, 2022]. Distinct from these works, we first introduce Beckman barycenter, a concept analogous to Wasserstein barycenter. We use proximal operator methods to solve for the barycenter. The barycenters obtained from the clean samples are used to train a pretrained adversarially robust network. We note that in the absence of adversarial samples in the training, the model would give a better clean accuracy but will suffer in terms of adversarial accuracy. Therefore, we use a pre-trained adversarially robust network to overcome this challenge. An abstract illustration of our method is given in Figure 1.

Beckman barycenter is obtained from input marginals via a non-linear interpolation. The input marginals are linearly transformed versions of the input and thus interfere with the adversarial noise. Using these marginals the barycenter generates a sample which is similar in appearance to the input and is closer in terms of class label. Thus, the class label is preserved when the input is a clean sample, whereas, the

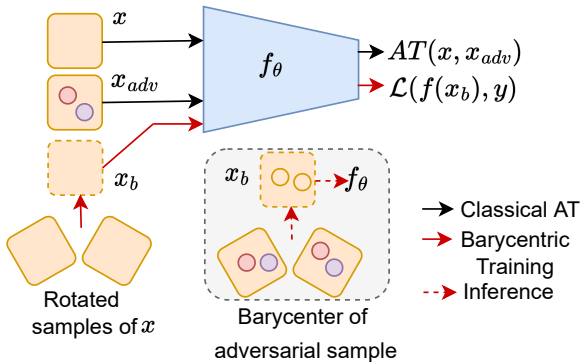


Figure 1: Illustration: Classical defense methods use Adversarial Training (AT) as a major defense technique. Our method obtains barycenter from rotated inputs and uses them for training the model using a cross-entropy loss. During inference time also we compute barycenter of the given sample. The dashed boundary of barycenter indicates that the barycenter is close to input samples in terms of appearance but there are some differences. In the computation of barycenter of adversarial sample, the barycenter shows the changes in same color as that of the background to imply that barycenter suppresses the adversarial noise.

adversarial noise gets suppressed when the input is an adversarial sample. Further, the network needs to be trained with barycenter of clean samples so as to correctly classify them. However, this training is cheap as a single epoch is sufficient. We prove our hypothesis using extensive qualitative and quantitative experiments.

2 Related Works

Adversarial Attacks Given an adversarial sample x with label y , a target network f parameterized by θ , the adversary tries to find x_{adv} by adding an adversarial noise such that the prediction $f_{\theta}(x_{adv}) \neq f_{\theta}(x) = y$. Some of the robust attacks are iterative FGSM [Kurakin et al., 2016], PGD [Madry et al., 2017], Carlini and Wagner attacks [Carlini and Wagner, 2017], Jacobian based attack [Papernot et al., 2016], physical attack Athalye [Athalye et al., 2018], and Autoattack [Croce and Hein, 2020]. These attacks are primarily focused in l_p domain.

Adversarial Defense In response to adversarial attacks, several defenses have been proposed. One of the best defense approach is adversarial training [Szegedy et al., 2013], [Goodfellow et al., 2014], [Moosavi-Dezfooli et al., 2016]. Madry et al. [Madry et al., 2017] formally studied adversarial training and proposed that such training allows network to defend well against first order adversary. Adversarial logit pairing uses a pair of logits from clean and adversarial examples to defend against adversarial samples [Kannan et al., 2018]. TRADES [Zhang et al., 2019] prove the bounds based on regularization term which minimizes the difference in prediction between clean and adversarial examples. In [Wong et al., 2020], authors proposed to effectively combine FGSM and random initialization to demonstrate better adversarial training. RST [Carmon et al., 2019] propose a self-training technique using unlabelled samples to improve the robust-

ness. Observing the correlation between flatness of weight loss landscape and adversarial robustness, Wu et al. proposed adversarial weight perturbation (AWP) to regularize the flatness of weight loss [Wu et al., 2020]. On similar lines, [Yu et al., 2022] propose a criterion called Loss Stationary Condition (LSC) for constrained perturbation, which regulates the weight perturbation to prevent overfitting. LBGAT [Cui et al., 2021] constrains the logits of a robust model, trained with adversarial examples, to be similar to the logits of a clean model trained on natural data.

While adversarial training uses all the samples, many techniques propose that naively using adversarial samples in adversarial training is not efficient. This primarily involves training the model with a weak attack first, and then gradually increasing the strength of the adversary - CAT [Cai et al., 2018], DART [Wang et al., 2019a], MART [Wang et al., 2019b], FAT [Zhang et al., 2020]. Aforementioned methods rely on pre-determined attack parameters for adversarial sample generation. However, this restricts the model’s robustness. To address this issue, LAS-AT [Jia et al., 2022] propose a framework for adversarial training that introduces the notion of learnable attack strategy. It is composed of two components: a target network that uses adversarial examples for training to improve robustness, and a strategy network that produces attack strategies to control adversarial sample generation. In similar spirit, A2 [Xu et al., 2022] and [Cheng et al., 2022] have also been proposed. A classical review of defense methods can be obtained in [Bai et al., 2021].

In a parallel line of defense works, input purification has also been explored. At the test time, these techniques try to remove the adversarial noise [Shi et al., 2021], TRADES_{SSL} [Mao et al., 2021], Hedge_{RST} [Wu et al., 2021]. Score based generative models such as [Yoon et al., 2021] and [Nie et al., 2022] have also been used to purify the images before sending them for classification.

Our work is inspired from two different theories, namely, OT barycenters and distributional robust optimization. We discuss these theories in the following.

Wasserstein Barycenter In the following we discuss Wasserstein distance and barycenter. Given probability distributions, $\mu_1, \mu_2 \in \Omega$, the Wasserstein distance is defined as,

$$\mathcal{W}(\mu_1, \mu_2) = \inf_{\Omega \times \Omega} \int c(x, y) \pi(x, y) dx dy, \quad (1)$$

$$s.t. \int_{\Omega} \pi(x, y) dx = \mu_1(x), \int_{\Omega} \pi(x, y) dy = \mu_2(y),$$

where the cost matrix $c(x, y) = \|x - y\|_1$ and π denotes the transport plan. This is also known as Earth Mover’s Distance (EMD). This form is also used to compute barycenter [Cuturi and Peyré, 2016] wherein the summation of Wasserstein distance between the barycenter and each input marginal is considered. However, barycenters are costly to compute and the best known complexity scales exponentially with the number of marginals [Fan et al., 2022].

EMD can also be represented as dual of the dual of Eq 1 in variational form popularly introduced by Beckman [Beck-

mann, 1952], [Li *et al.*, 2018], [Lee *et al.*, 2020],

$$\begin{aligned} \mathcal{W}(\boldsymbol{\mu}_1, \boldsymbol{\mu}_2) &= \inf_{\mathbf{M}} \int_{\Omega} \|\mathbf{M}\| & (2) \\ \text{s.t. } \operatorname{div}(\mathbf{M}) + \boldsymbol{\mu}_1 - \boldsymbol{\mu}_2 &= 0 \\ \mathbf{M} \cdot \mathbf{n} &= 0 \quad \forall x \in \partial\Omega; n \text{ is normal to } \partial\Omega \end{aligned}$$

Under appropriate discretization, $\mathbf{M} = (\mathbf{M}_x, \mathbf{M}_y)$, $\mathbf{M} \in \mathcal{R}^{n \times 2}$ is flux vector satisfying zero flux boundary conditions. $\boldsymbol{\mu}_1, \boldsymbol{\mu}_2 \in \mathcal{R}^n$, and,

$\operatorname{div}(\mathbf{M}) = (\mathbf{M}_x[i, j] - \mathbf{M}_x[i-1, j]) + (\mathbf{M}_y[i, j] - \mathbf{M}_y[i, j-1])$ and the zero-flux boundary conditions mean that $\mathbf{M}_x[i, j] = \mathbf{M}_y[i, j] = 0$ outside the boundary. Eq 2 is favorable compared to Eq 1 as it reduces the complexity from $\mathcal{O}(n^2)$ to $\mathcal{O}(n)$ [Li *et al.*, 2018]. Motivated by the recent developments of OT barycenters, we make use of Eq 2 to propose Beckman barycenter as they can be efficiently solved using well known techniques like [Goldstein and Osher, 2009], [Chambolle and Pock, 2011].

DRO One of the influential works in DRO was proposed by Scarf [Scarf, 1957]. Following this work, significant research has been done in this field [Ben-Tal *et al.*, 2009], [Duchi *et al.*, 2021], [Staib and Jegelka, 2017]. DRO aims to address the problem of uncertainty or shift in the data distribution that can arise due to measurement errors and admits a solution for the worst case scenario. Let $\mathcal{L}(\boldsymbol{\theta}, \mathbf{x})$ be the loss function where $\boldsymbol{\theta}$ are network parameters. Then, DRO solves for,

$$\inf_{\boldsymbol{\theta}} \sup_{\mathcal{Q} \in \mathcal{Q}} \mathbb{E}_{\mathcal{Q}} \mathcal{L}(\boldsymbol{\theta}, \mathbf{x}) \quad (3)$$

Here, \mathcal{Q} is the distribution against which DRO minimizes the loss. For instance, \mathcal{Q} can be considered as a distribution set which contains perturbations of input samples \mathbf{x} . Here we note that adversarial training can be considered to be a specific instance of DRO wherein the distribution \mathcal{Q} is drawn from adversarial samples. In our case, we consider the barycenters as the samples drawn from the distribution \mathcal{Q} and thus provide robustness against perturbed samples.

2.1 Proposed Algorithm

In this work, we propose a novel Beckman barycenter formulation and derive the barycenter analytically. We use the barycenter to demonstrate that it can be applied for adversarial defense. We first obtain the barycenter using the marginals from the given input image and then train the network using barycenter.

While OT barycenters are a good choice for the distribution \mathcal{Q} in Eq 3, computing OT barycenter suffers from high complexity and exponentially increases with the number marginals [Fan *et al.*, 2022]. To counter this high complexity challenge, we first discuss an analogous barycenter problem by building upon the formulation given in Eq 2,

$$\begin{aligned} \inf_{\mathbf{M}_1, \mathbf{M}_2, \mathbf{r}_1, \mathbf{r}_2, \boldsymbol{\mu}} & \|\mathbf{M}_1\|_{2,1} + \|\mathbf{M}_2\|_{2,1} + \alpha(\|\mathbf{r}_1\|_1 & (4) \\ & + \|\mathbf{r}_2\|_1) + \beta\|\boldsymbol{\mu}\|_1 \\ \text{s.t. } \operatorname{div}(\mathbf{M}_1) + \boldsymbol{\mu}_1 - \boldsymbol{\mu} &= \mathbf{r}_1 \\ \operatorname{div}(\mathbf{M}_2) + \boldsymbol{\mu}_2 - \boldsymbol{\mu} &= \mathbf{r}_2 \end{aligned}$$

where, $\mathbf{r}_1, \mathbf{r}_2, \boldsymbol{\mu} \in \mathcal{R}^n$. Our formulation is loosely inspired from the Beckman OT formulation that is given in [Li *et al.*, 2018], [Lee *et al.*, 2020]. There are notable changes in Eq 4 from Eq 2. First we solve for Beckman barycenter $\boldsymbol{\mu}$ in addition to other variables. Similar to Wasserstein barycenter which acts as a representative of marginals using Wasserstein metric, the Beckman barycenter $\boldsymbol{\mu}$ minimizes the flux with respect to input marginals $\boldsymbol{\mu}_1$ and $\boldsymbol{\mu}_2$. In our experiments, these marginals are obtained by rotating the input image with $\pm 4^\circ$. Second, the variables \mathbf{r}_1 and \mathbf{r}_2 allow the mass to be created or destroyed [Lee *et al.*, 2020] and the regularization over $\mathbf{r}_1, \mathbf{r}_2$ and $\boldsymbol{\mu}$ ensure that these variable do not take arbitrarily large values. Third, Eq 4 can be easily converted to Lagrange formulation and solved in linear time using primal-dual method of Chambolle and Pock [Chambolle and Pock, 2011].

In order to make the objective strongly convex, we first apply proximal operators. The l_2 regularizer makes the objective strongly convex. Using the proximal operator,

$$\begin{aligned} \inf_{\mathbf{M}_1, \mathbf{M}_2, \mathbf{r}_1, \mathbf{r}_2, \boldsymbol{\mu}'_1, \boldsymbol{\mu}'_2, \boldsymbol{\mu}} & \|\mathbf{M}_1\|_{2,1} + \|\mathbf{M}_2\|_{2,1} + \alpha(\|\mathbf{r}_1\|_1 & (5) \\ & + \|\mathbf{r}_2\|_1) + \frac{1}{2\rho}(\|\boldsymbol{\mu}'_1 - \boldsymbol{\mu}_1\|_2 + \|\boldsymbol{\mu}'_2 - \boldsymbol{\mu}_2\|_2) + \beta\|\boldsymbol{\mu}\|_1 \\ \text{s.t. } \operatorname{div}(\mathbf{M}_1) + \boldsymbol{\mu}'_1 - \boldsymbol{\mu} &= \mathbf{r}_1 \\ \operatorname{div}(\mathbf{M}_2) + \boldsymbol{\mu}'_2 - \boldsymbol{\mu} &= \mathbf{r}_2 \end{aligned}$$

The Lagrangian of Eq 5 is given as,

$$\begin{aligned} \inf_{\mathbf{M}_1, \mathbf{M}_2, \mathbf{r}_1, \mathbf{r}_2, \boldsymbol{\mu}'_1, \boldsymbol{\mu}'_2, \boldsymbol{\mu}} & \|\mathbf{M}_1\|_{2,1} + \|\mathbf{M}_2\|_{2,1} + \alpha(\|\mathbf{r}_1\|_1 & (6) \\ & + \|\mathbf{r}_2\|_1) + \frac{1}{2\rho}(\|\boldsymbol{\mu}'_1 - \boldsymbol{\mu}_1\|_2 + \|\boldsymbol{\mu}'_2 - \boldsymbol{\mu}_2\|_2) + \beta\|\boldsymbol{\mu}\|_1 \\ & + \sum_i \langle \boldsymbol{\lambda}_i, \operatorname{div}(\mathbf{M}_i) + \boldsymbol{\mu}'_i - \boldsymbol{\mu} - \mathbf{r}_i \rangle \end{aligned}$$

Eq 6 can be solved using first-order primal dual method of Chambolle and Pock [Chambolle and Pock, 2011]¹.

$$\begin{aligned} \mathbf{M}_i^{t+1} &\leftarrow \arg \min_{\mathbf{M}_i} \|\mathbf{M}_i\|_{2,1} + \langle \boldsymbol{\lambda}_i, \operatorname{div}(\mathbf{M}_i) + \boldsymbol{\mu}'_i - & \\ & \boldsymbol{\mu} - \mathbf{r}_i \rangle + \frac{1}{2\tau_1} \|\mathbf{M}_i - \mathbf{M}_i^t\|_2 \quad \forall i = \{1, 2\} \\ \boldsymbol{\mu}'_i^{t+1} &\leftarrow \arg \min_{\boldsymbol{\mu}'_i} \frac{1}{2\tau_1} (\|\boldsymbol{\mu}'_i - \boldsymbol{\mu}_i\|_2) + \langle \boldsymbol{\lambda}_i, \boldsymbol{\mu}'_i \rangle & \\ & + \frac{1}{2\tau_1} \|\boldsymbol{\mu}'_i - \boldsymbol{\mu}'_i^t\|_2 \\ \mathbf{r}_i^{t+1} &\leftarrow \arg \min_{\mathbf{r}_i} \alpha \|\mathbf{r}_i\|_1 + \langle \boldsymbol{\lambda}_i^t, -\mathbf{r}_i \rangle + \frac{1}{2\tau_1} \|\mathbf{r}_i - \mathbf{r}_i^t\|_2 & \\ \boldsymbol{\mu}^{t+1} &\leftarrow \arg \min_{\boldsymbol{\mu}} \|\boldsymbol{\mu}\|_1 + \langle \boldsymbol{\lambda}_i^t, -\boldsymbol{\mu} \rangle + \frac{1}{2\tau_1} \|\boldsymbol{\mu} - \boldsymbol{\mu}^t\|_2 & \\ \boldsymbol{\lambda}_i^{t+1} &\leftarrow \arg \max_{\boldsymbol{\lambda}_i} \langle \boldsymbol{\lambda}_i, \boldsymbol{\kappa}^{t+1} \rangle - \frac{1}{2\tau_2} \|\boldsymbol{\lambda}_i - \boldsymbol{\lambda}_i^t\|_2, & \end{aligned}$$

¹We use similar notations to that of [Li *et al.*, 2018], [Chambolle and Pock, 2011] for consistency and simplicity.

where, $\kappa^{t+1} = 2(\text{div}(\mathbf{M}_i)^{t+1} + \mu_i'^{t+1} - \mathbf{r}_i^{t+1}) - (\text{div}(\mathbf{M}_i)^t + \mu_i'^t - \mathbf{r}_i^t)$.

We now discuss the solution of each individual optimization.

Solving for \mathbf{M}_i : The rows \mathbf{m}_{ij} of \mathbf{M}_i can be expressed and solved using l_{21} norm shrinkage operator,

$$\mathbf{m}_{ij}^{t+1} \leftarrow \text{shrink}_{\tau_1}^{l_2}(\mathbf{m}_{ij}^t - \tau_1 \text{div}^*(\lambda_i^t)_j) \quad (7)$$

Here, div^* denotes the adjoint of div operator, and $\text{shrink}_{\tau_1}^{l_2} \boldsymbol{\eta} = \max(\|\boldsymbol{\eta}\|_2 - \tau_1, 0) \odot \frac{\boldsymbol{\eta}}{\|\boldsymbol{\eta}\|_2}$. “ \odot ” denotes the Hadamard product.

Solving for μ_i' :

$$\mu_i'^{t+1} \leftarrow \max\{0, \frac{\rho\tau_1}{1 + \rho\tau_1} \mu_i' + \frac{1}{1 + \rho\tau_1} (\mu_i'^t - \tau_1 \lambda_i^t)\}, \quad (8)$$

Solving for \mathbf{r}_i : We use an l_1 shrinkage operator.

$$\mathbf{r}_i^{t+1} \leftarrow \text{shrink}_{\alpha\tau_1}^{l_1}(\mathbf{r}_i^t + \tau_1 \lambda_i^t) \quad (9)$$

Here, $\text{shrink}_{\alpha\tau_1}^{l_1}(\boldsymbol{\eta}) = \text{sign}(\boldsymbol{\eta}) \odot \max(\|\boldsymbol{\eta}\| - \alpha\tau_1, 0)$.

Solving for barycenter μ :

$$\mu^{t+1} \leftarrow \text{shrink}_{\beta\tau_1}^{l_1}(\mu^t + \tau_1(\lambda_1^t + \lambda_2^t)) \quad (10)$$

Solving for λ :

$$\lambda_i^{t+1} \leftarrow \lambda_i^t + \tau_2 \kappa^{t+1} \quad (11)$$

2.2 Toy example

We demonstrate the barycenter computation using a Gaussian image in Figure 2. The barycenter of clean samples, sample with random noise and adversarial sample are shown. As we see, for the clean case the barycenter is very similar to that of the original image. In the second column where random noise is added, the barycenter reduces the noise. Similar effect is also seen for the case where adversarial noise is present. This indicates that non-linear interpolation of barycenter suppresses the adversarial noise.

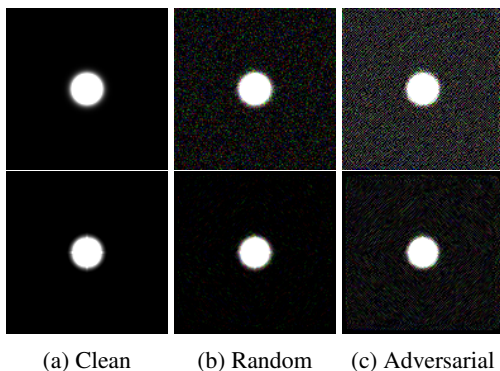


Figure 2: Top: Clean image, noisy image, adversarial image. Bottom: Barycenter of clean image, noisy image, adversarial image.

2.3 Training

Let a model be given by f_θ , the barycenter of clean samples be denoted by \mathbf{x} and its labels as y . We then optimize the following loss

$$\arg \min_{\theta} \frac{1}{n} \sum_{i=1}^n \mathcal{L}_{CE}(f_\theta(\mathbf{x}_i), \mathbf{y}_i)$$

where \mathcal{L}_{CE} is the cross-entropy loss. We would like to emphasize that we do not perform adversarial training. Instead we use an adversarially pretrained model. Thus, f_θ is an adversarial robust model and our training further enhances the robustness. We also note that this optimization falls under DRO as the samples used are barycenters which belong to the distribution \mathcal{Q} .

2.4 Theoretical analysis

We first present a convergence analysis of Eq 6.

Theorem 1. Let $\tau_1 \tau_2 (\lambda_{\max}(\nabla^2) + 3) < 1$, where $\lambda_{\max}(\nabla^2)$ denotes the largest eigenvalue of discrete Laplacian operator $\nabla^2 = \mathbf{D}\mathbf{D}^\top$, where \mathbf{D} is the matrix representing div operator. Then, the iterations $\mathbf{M}_i^t, \mu_i'^t, \mu^t, \mathbf{r}_i^t, \lambda_i^t$ converge to the saddle point solution of the Lagrangian $\mathbf{M}_i^*, \mu_i^*, \mu^*, \mathbf{r}_i^*, \lambda_i^*$.

Proof: Let $\mathbf{u} = \{\mathbf{M}_1, \mathbf{M}_2, \mu_2, \mu, \mathbf{r}\}$. Then, we write Eq 6 as

$$\mathcal{L}(\mathbf{u}, \boldsymbol{\lambda}) = \mathcal{G}(\mathbf{u}) + \langle \boldsymbol{\lambda}, \tilde{\mathbf{K}}\mathbf{b} \rangle$$

where $\boldsymbol{\lambda} = [\lambda_1; \lambda_2]$, $\mathbf{K} = [\mathbf{D}, \mathbf{I}, -\mathbf{I}, -\mathbf{I}]$, $\tilde{\mathbf{K}} = [\mathbf{K}, \mathbf{0}; \mathbf{0}, \mathbf{K}]$, $\mathbf{b} = [\mathbf{b}_1; \mathbf{b}_2]$, $\mathbf{b}_1 = [\text{vec}(\mathbf{M}_1); \mu_1'; \mu; \mathbf{r}_1]$; $\mathbf{b}_2 = [\text{vec}(\mathbf{M}_2); \mu_2'; \mu; \mathbf{r}_2]$. The function $\mathcal{G} = \|\mathbf{M}_1\|_{2,1} + \|\mathbf{M}_2\|_{2,1} + \alpha(\|\mathbf{r}_1\|_1 + \|\mathbf{r}_2\|_1) + \frac{1}{2\rho}(\|\mu_1' - \mu_1\|_2 + \|\mu_2' - \mu_2\|_2) + \beta\|\mu\|_1$ is convex and $\tilde{\mathbf{K}}$ is a linear operator. These conditions satisfy Theorem 1 of [Chambolle and Pock, 2011]. If $\lambda_{\max}(\nabla^2)$ is the max eigenvalue of $\mathbf{D}\mathbf{D}^\top$, then the max eigenvalue of $[\mathbf{D}, \pm\mathbf{I}][\mathbf{D}, \pm\mathbf{I}]^\top$ is $\lambda_{\max}(\nabla^2) + 1$. Similarly, for $\mathbf{K}\mathbf{K}^\top$, it is $\lambda_{\max}(\nabla^2) + 3$. Since $\tilde{\mathbf{K}}$ is obtained from \mathbf{K} by padding zeros only, $\tilde{\mathbf{K}}$ has the same max eigenvalue as that of \mathbf{K} . Further, since $\|\tilde{\mathbf{K}}\tilde{\mathbf{K}}^\top\|_2^2 \geq \lambda_{\max}(\tilde{\mathbf{K}}\tilde{\mathbf{K}}^\top) = \lambda_{\max}(\nabla^2) + 3$, we can also write the convergence criteria as $\tau_1 \tau_2 \|\tilde{\mathbf{K}}\tilde{\mathbf{K}}^\top\|_2^2 < 1$.

Since we solve for the Lagrangian dual function, we analyse the primal dual gap which is given as [Jacobs et al., 2019]

$$\mathbb{G}(\mathbf{u}, \boldsymbol{\lambda}) = \sup_{\|\boldsymbol{\lambda}' - \boldsymbol{\lambda}_0\| \leq R_1} \mathcal{L}(\mathbf{u}, \boldsymbol{\lambda}') - \inf_{\|\mathbf{u}' - \mathbf{u}_0\| \leq R_2} \mathcal{L}(\mathbf{u}', \boldsymbol{\lambda})$$

Theorem 2. Suppose the step sizes τ_1 and τ_2 satisfy $\tau_1 \tau_2 \|\tilde{\mathbf{K}}\tilde{\mathbf{K}}^\top\|_2^2 < 1$. Let $\mathbf{u}^N = \frac{1}{N} \sum_{n=1}^N \mathbf{u}_n$ and $\boldsymbol{\lambda}^N = \frac{1}{N} \sum_{n=1}^N \boldsymbol{\lambda}_n$, where \mathbf{u}_n and $\boldsymbol{\lambda}_n$ are sequences generated from Eqns 7 - 11. Then after N iterations, we have,

$$\mathbb{G}(\mathbf{u}, \boldsymbol{\lambda}) \leq \sup_{\mathbf{u}, \boldsymbol{\lambda}} \frac{1}{2N} \left(\frac{\|\mathbf{u} - \mathbf{u}_0\|_2}{\tau_1} + \frac{\|\boldsymbol{\lambda} - \boldsymbol{\lambda}_0\|_2}{\tau_2} \right)$$

This rate is similar to convergence rates in gradient descent and shows that the gap converges with rate $\mathcal{O}(1/N)$. For brevity, we omit the proof and it can be derived as an extension of Theorem 1 [Chambolle and Pock, 2011].

2.5 Mutual Information

In order to understand the underlying reason behind the performance of our method, we provide more insights using mutual information (MI). We first note that the MI between two random variables is given by $\mathcal{I}(X, y) = \mathcal{H}(\mathcal{P}(y)) - E_{P(x)} [\mathcal{H}(\mathcal{P}(y|X))]$. In our case, we take the random variables as model parameters θ and softmax output y . Then, given a sample x and dataset \mathcal{D} ,

$$\mathcal{I}(\theta, y|\mathcal{D}, x) = \mathcal{H}(p(y|x, \mathcal{D})) - E_{p(\theta|\mathcal{D})} \mathcal{H}(p(y|x, \theta)) \quad (12)$$

Eq 12 measures the information shared between θ and y . A tractable way of computing $\mathcal{I}(\theta, y|\mathcal{D}, x)$ is given in [Smith and Gal, 2018], [Houlsby et al., 2011].

$$\mathcal{I}(\theta, y|\mathcal{D}, x) = \frac{1}{C} \sum_{j=1}^C \frac{1}{n} \sum_{i=1}^n (p_{ij} - \hat{p})^2 \quad (13)$$

where, $\hat{p} \in [0, 1]^C$ is computed as the mean of all softmax probabilities, C is the number of classes, $\mathbf{p}_i \in [0, 1]^C$, $p_{ij} \in [0, 1]$ denotes the softmax probability for a particular class j . A higher \mathcal{I} indicates that knowing θ (or y) gives a higher information about y (or θ). In other words, the model will perform better if the mutual information is high.

In addition, we also compute MI between the predictions for the following two cases - (i) clean test set and adversarial test set, and (ii) barycenter of clean test set and barycenter of adversarial test set using [Ji et al., 2019]. Given a model f parameterised by θ , clean sample \mathbf{x}_i and its adversarial counterpart \mathbf{x}'_i , the joint probability distribution between natural and adversarial samples is given by the following $C \times C$ matrix,

$$\mathcal{I}(f(\mathbf{x}_i, \theta), f(\mathbf{x}'_i, \theta)) = \sum_{y=1}^C \sum_{y'=1}^C \mathcal{P}_{yy'} \ln \frac{\mathcal{P}_{yy'}}{\mathcal{P}_y \mathcal{P}_{y'}} \quad (14)$$

where, $\mathcal{P}_{yy'}$ is given as,

$$\mathcal{P}_{yy'} = \frac{1}{n} \sum_{i=1}^n f(\mathbf{x}_i, \theta) f(\mathbf{x}'_i, \theta)^\top \quad (15)$$

and the marginals $\mathcal{P}_y, \mathcal{P}_{y'}$ are obtained by row and column sum of $\mathcal{P}_{yy'}$. A higher value of $\mathcal{I}(\cdot, \cdot)$ indicates that knowing about clean samples gives a higher amount of information about the adversarial samples.

3 Experiments

We present elaborate experimental results on CIFAR-10, CIFAR-100 and Tiny ImageNet. We use strong baselines of LAS [Jia et al., 2022], LBGAT [Cui et al., 2021], PGD-AT [Madry et al., 2017], TRADES [Zhang et al., 2019], RST [Carmon et al., 2019]. We compare against several popular adversarial training models, MART [Wang et al., 2019b], AWP-A2 [Xu et al., 2022], RST-RWT [Yu et al., 2022], TRADES_{AWP} [Wu et al., 2020], AWP [Wu et al., 2020], LAS_{AT}, LAS_{TRADES}, LAS_{AWP} [Jia et al., 2022]. We also compare with adaptive test time defenses Hedge_{RST} [Wu et al., 2021] and TRADES_{SSL} [Mao et al., 2021]. In the Tables, we use “+B” to indicate the results obtained using our approach.

3.1 Implementation details

In case of CIFAR10 and CIFAR100, WideResNet34-10 is used and for Tiny ImageNet PreActResnet18 is used. Additionally, we evaluate on CIFAR-10 with WideResNet28-10, WideResNet32-10, WideResNet70-16 and on CIFAR-100 with WideResNet34-20. We use these models for a fair comparison with existing works as these models are widely used for adversarial defense evaluation. We evaluate against different attacks namely FGSM, PGD-10, PGD-20, CW, and AA using l_∞ attack with $\epsilon = 8/255$. Our evaluation protocols are similar to the protocols given in [Zhang et al., 2019], [Jia et al., 2022]. We would like to emphasize that we use the checkpoints from the baseline models and perform a single epoch training using clean barycenters. Upon increasing the number of epochs, the clean accuracy improves, however, the adversarial accuracy becomes comparable to that of baseline and further increasing epochs leads to subsequent drop in accuracy against adversarial samples. We use SGD optimizer with a learning rate of 1e-4, momentum = 0.9 without any weight decay.

In order to compute the barycenter, we set $\rho = 5e-1$, $\tau_1 = 1e-1$, $\tau_2 = \alpha = \beta = 1$ and iterations is set to 200. While one can also attack the barycenter, we give experiments for the case where the clean image is attacked. This is because the barycenter itself lies at an ϵ which is greater than attacker’s budget. Thus attacking barycenter has little incentive as in that case the attacked image will lie at an ϵ outside the given $\epsilon = 8/255$ for the l_∞ attack.

3.2 Comparison on CIFAR-10

In Table 1, we observe that clean performance is better for the models trained with barycenters - TRADES_{AWP}+B, LBGAT+B, LAS_{TRADES}+B and RST+B. Amongst WRN-28-10 models, RST has the best clean performance and our method enhances it by 1%. In PGD-10, there is a rise of 2.57%. In case of AA, there is a boost of 6.49%.

In case of WRN-34-10, LAS_{AT}+B shows a huge boost of 10% under AA. Further, LAS_{AWP}+B shows the best performance under PGD-10, PGD-20 and CW attack amongst WRN-34-10 models. Under AA it shows an improvement of 7.71%.

Comparison with Adversarial Purification models Our RST+B model outperforms Hedge_{RST}* under all the cases. Against AA, our approach gives 3.1% higher accuracy compared to Hedge_{RST}*. We also see that compared to TRADES_{SSL}, TRADES_{AWP} has a better performance.

3.3 Comparison on CIFAR-100

In Table 2, we observe that our method gives a significant boost under all the cases. In case of strong baseline LAS_{AWP}, our method increases the performance by 0.85% under clean accuracy. For PGD-20, there is a rise of 0.91%. In case of CW, there is an increase of 18.35%. In other models such as LBGAT, we see a rise of 5.4% in clean accuracy.

3.4 Comparison on Tiny ImageNet

We present the results in Table 3. In comparison to baselines, our method shows significant improvement in all cases. For

Table 1: CIFAR-10. * indicates that the model uses WRN-28-10. **Bold** font is used to indicate the best performance amongst WRN-34-10 and **Red** color font is used to indicate the best performance amongst WRN-28-10.

Method	Clean	PGD10	PGD20	CW	AA
Adversarial Training					
PGD-AT	85.17	56.07	55.08	53.91	51.69
TRADES	85.72	56.75	56.10	53.87	53.40
MART	84.17	58.98	58.56	54.58	51.10
AWP-A2	87.54	-	59.50	57.42	54.86
RST-RWT*	88.87	-	64.11	62.03	60.36
Adversarial Purification					
TRADES _{SSL}	82.12	-	-	-	60.67
Hedge _{RST} *	88.64	-	-	73.89	63.10
Adversarial and Barycentric Training					
TRADES _{AWP}	85.36	59.58	59.25	57.07	56.17
+B	87.32	62.60	62.32	75.85	65.32
LBGAT	88.22	56.25	54.60	54.29	52.23
+B	88.38	59.28	58.43	74.61	61.22
LAS _{AT}	86.23	57.11	56.41	55.54	53.58
+B	86.21	61.08	60.64	74.09	63.59
LAS _{TRADES}	85.24	57.66	57.07	55.45	54.15
+B	86.15	60.32	60.03	73.75	63.43
LAS _{AWP}	87.74	61.09	60.16	58.22	55.52
+B	87.45	63.66	61.16	74.81	63.23
RST*	89.69	63.48	62.51	61.06	59.71
+B*	90.68	65.12	64.38	77.08	66.20

LAS_{AWP}, our method improves the performance under clean samples by 1.65%. In case of PGD-50, our method shows a rise of 1.28%, and in case of CW attack, our method almost doubles the accuracy. Under AA, LAS_{TRADES} observes a maximum performance rise by 11.51%.

3.5 Comparison with Curriculum based AT

In Table 4, we compare against curriculum based AT methods like CAT [Cai *et al.*, 2018], FAT [Zhang *et al.*, 2020] and DART [Wang *et al.*, 2019a]. Under FGSM, PGD-20 and CW, our model shows a huge improvement. In FGSM, our model gives a boost of 4.46% over FAT. In PGD-20 the boost is 10.89% and in CW there is a rise of 24.54%. In case of clean samples, we see that the accuracy of FAT+B compared to FAT is less. This may be due to the fact that FAT employs curriculum learning in the training whereas our method does not use curriculum learning.

3.6 Analysis using Deeper and Wider Models

We use WRN-70-16 and WRN-34-20 to analyse the effect when the models get deeper and wider. In particular, for clean samples, we can observe that the deeper and wider models give a better boost. In CIFAR-10, WRN-70-16 gives 88.87% for clean samples which is 3.21% better than LAS_{AWP} model's 85.66%. In contrast, for WRN-34-10, our method gives accuracy similar to that of LAS_{AWP}.

In CIFAR-100, our method boosts the performance by 8.34% under AA. In other cases also we see that the barycenters improve the performance by a significant margin.

Table 2: CIFAR-100 WRN-34-10.

Method	Clean	PGD-10	PGD-20	CW
PGD-AT	60.89	32.19	31.69	30.10
TRADES	58.61	29.20	28.66	27.05
TRADES _{AWP}	60.17	33.81	33.6	57.07
+B	63.67	36.34	36.15	51.92
LBGAT	60.64	35.13	34.53	30.65
+B	66.04	36.29	36.01	52.92
LAS _{AT}	61.8	33.27	32.83	31.12
+B	62.45	36.60	36.17	49.60
LAS _{TRADES}	60.62	32.82	32.51	29.51
+B	62.58	35.22	34.96	50.99
LAS _{AWP}	64.89	37.11	36.36	33.92
+B	65.50	37.55	37.27	52.27

Table 3: Tiny ImageNet PreActResNet18.

Method	Clean	PGD-50	CW	AA
LAS _{AT}	44.86	22.16	18.54	16.74
+B	45.12	24.54	37.14	27.78
LAS _{TRADES}	41.38	18.36	14.50	14.08
+B	43.07	19.25	35.13	25.59
LAS _{AWP}	45.26	23.42	19.88	18.42
+B	46.91	24.70	37.93	27.00

3.7 TSNE

In Figure 3, we show the tsne plots for MNIST testset with classes 0 and 1. Here, we use a weak MNIST model which has only two dimensions before the classification layer. We deliberately chose a weak model so that we can easily show the effect in low dimensions. Though higher dimensions could be taken, the effect cannot be easily seen due to a highly non-linear transformation from high to low dimension of tsne. We can see that the two clusters yellow and purple are well separated for clean and barycenters of clean images. In case of adversarial samples, the points overlap on each other. However, when we take barycenter of adversarial samples, we again see that the clusters are well separated, similar to the case of clean images. Thus, it is evident that the barycenter nullifies the effect of adversarial noise.



(a) Clean (b) Barycenter (c) Attacked (d) Adv.+Bary.

Figure 3: Left to right: Plot of 2D features of Clean image, Barycenter of clean image, Attacked image, Barycenter of adversarial image. MNIST model obtains 51% accuracy and has only 2D feature vector before the classification layer.

3.8 Mutual Information

In Table 6, we present the study of mutual information. We use LAS_{AT} and LAS_{TRADES} on CIFAR-10. The MI is com-

Table 4: CIFAR-10 WRN-32-10.

Method	Clean	FGSM	PGD-20	CW
CAT	77.43	57.17	46.06	42.48
DART	85.03	63.53	48.70	47.27
FAT	89.34	65.52	46.13	46.82
+B	84.59	69.98	57.02	71.36

Table 5: CIFAR-10 (C-10) WRN-70-16 and CIFAR-100 (C-100) WRN-34-20.

Dataset	Method	Clean	FGSM	CW	AA
C-10	LAS _{AWP}	85.66	70.25	58.44	57.61
	+B	88.87	74.04	75.40	62.54
C-100	LBGAT	62.55	43.16	31.72	31.92
	+B	66.86	50.92	54.19	40.26

puted using Eq 12 and Eq 14. Here we note that the MI for LAS_{AT}+B is more for training set compared to that of LAS_{AT}. This indicates that the information available about the labels given the model parameters is high and in turn gives a better clean accuracy. In case of adversarial samples too, we see that the MI is higher for our case. This indicates that the model has better prediction for these samples. Further, the MI for test set is smaller compared to training set which is expected as the model carries more information about train set compared to test set.

Table 6: CIFAR-10 WRN-34-10.

Method	Train	Test	FGSM	CW
LAS _{AT}	0.029	0.026	0.020	0.019
+B	0.034	0.029	0.023	0.022
LAS _{TRADES}	0.048	0.040	0.033	0.032
+B	0.054	0.045	0.037	0.036

In Table 7, we present the results obtained using Eq 14. We observe that for the model trained with barycenter, the MI is higher between the barycenter of clean and adversarial samples. Thus, the model does better on barycenter of adversarial samples compared to baseline LAS_{AT} and TRADES_{AWP}. This is consistent across FGSM, PGD-10 and CW attacks.

3.9 Sensitivity to Barycenter Parameters

In Figure 4, we demonstrate the sensitivity to different parameters involved in the computation of barycenter. In the top row, we fix the number of iterations to 200 and $\tau_1 = 1e - 1$. Here we observe that increasing τ_2 makes the barycenter brighter. In the second row, increasing τ_1 makes the barycenter darker. Decreasing iterations has a similar effect in the last row. We see that unless there is a change of order of magnitude, the appearance does not substantially change. Thus, our proposed Beckman barycenter is robust with respect to the parameter settings.

The Figure 5 demonstrates a visualization of clean image, its barycenter, attacked image and its barycenter. The difference between them is imperceptible except for the black portion in the border for barycenters. This arises due to interpolation of the images from rotation.

Table 7: Mutual Information for CIFAR-10 WRN-34-10.

Method	FGSM	PGD-10	CW
LAS _{AT}	0.218	0.198	0.203
+B	0.275	0.241	0.264
LAS _{TRADES}	0.576	0.554	0.563
+B	0.629	0.572	0.618



Figure 4: Top row: Blue boundary represent the given image. Barycenter for iterations = 200, $\tau_1 = 1e - 1$, $\tau_2 = 1, 1e-1, 1e-2, 1e-3$. Second: barycenter for iterations = 200, $\tau_1=1, 1e-1, 1e-2, 1e-3$, $\tau_2 = 1$. Third: iterations = 200, 100, 50, 10, $\tau_1=1e-1$, $\tau_2=1$. The red boundary indicates the images obtained from default settings of the parameter which are used for all experiments.

4 Conclusion

In this work we introduce Beckman barycenter analogous to Wasserstein barycenter. We use the Beckman OT formulation and analytically solve for the barycenter. Defining the barycenter using Beckman OT also has the advantage that the computational tools to obtain barycenter are well known and efficient. This overcomes the complexity in solving Wasserstein barycenters. Further, we show that barycenter can be used for enhancing the performance of adversarially trained models. Our training is very efficient as we only need a single epoch. Experimental analysis demonstrates state-of-art results against different attacks.

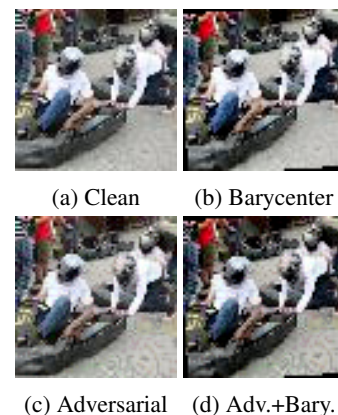


Figure 5: Illustration of barycenters from Tiny ImageNet.

References

- [Agueh and Carlier, 2011] Martial Agueh and Guillaume Carlier. Barycenters in the wasserstein space. *SIAM Journal on Mathematical Analysis*, 43(2):904–924, 2011.
- [Athalye *et al.*, 2018] Anish Athalye, Logan Engstrom, Andrew Ilyas, and Kevin Kwok. Synthesizing robust adversarial examples. In *ICML*, pages 284–293. PMLR, 2018.
- [Bai *et al.*, 2021] Tao Bai, Jinqi Luo, Jun Zhao, Bihan Wen, and Qian Wang. Recent advances in adversarial training for adversarial robustness. In *IJCAI*, 2021.
- [Beckmann, 1952] Martin Beckmann. A continuous model of transportation. *Econometrica: Journal of the Econometric Society*, pages 643–660, 1952.
- [Ben-Tal *et al.*, 2009] Aharon Ben-Tal, Laurent El Ghaoui, and Arkadi Nemirovski. *Robust optimization*, volume 28. Princeton university press, 2009.
- [Cai *et al.*, 2018] Qi-Zhi Cai, Min Du, Chang Liu, and Dawn Song. Curriculum adversarial training. *arXiv preprint arXiv:1805.04807*, 2018.
- [Carlini and Wagner, 2017] Nicholas Carlini and David Wagner. Towards evaluating the robustness of neural networks. In *Symposium on security and privacy*, pages 39–57, 2017.
- [Carmon *et al.*, 2019] Yair Carmon, Aditi Raghunathan, Ludwig Schmidt, John C Duchi, and Percy S Liang. Unlabeled data improves adversarial robustness. *NeurIPS*, 2019.
- [Chambolle and Pock, 2011] Antonin Chambolle and Thomas Pock. A first-order primal-dual algorithm for convex problems with applications to imaging. *Journal of mathematical imaging and vision*, 40(1):120–145, 2011.
- [Cheng *et al.*, 2022] Minhao Cheng, Qi Lei, Pin-Yu Chen, Inderjit Dhillon, and Cho-Jui Hsieh. Cat: Customized adversarial training for improved robustness. In *IJCAI*, 2022.
- [Croce and Hein, 2020] Francesco Croce and Matthias Hein. Reliable evaluation of adversarial robustness with an ensemble of diverse parameter-free attacks. In *ICML*, pages 2206–2216. PMLR, 2020.
- [Cui *et al.*, 2021] Jiequan Cui, Shu Liu, Liwei Wang, and Jiaya Jia. Learnable boundary guided adversarial training. In *ICCV*, pages 15721–15730, 2021.
- [Cuturi and Doucet, 2014] Marco Cuturi and Arnaud Doucet. Fast computation of wasserstein barycenters. In *ICML*, pages 685–693. PMLR, 2014.
- [Cuturi and Peyré, 2016] Marco Cuturi and Gabriel Peyré. A smoothed dual approach for variational wasserstein problems. *SIAM Journal on Imaging Sciences*, 9(1):320–343, 2016.
- [Cuturi, 2013] Marco Cuturi. Sinkhorn distances: Light-speed computation of optimal transport. *NeurIPS*, 26:2292–2300, 2013.
- [Duchi *et al.*, 2021] John C Duchi, Peter W Glynn, and Hongseok Namkoong. Statistics of robust optimization: A generalized empirical likelihood approach. *Mathematics of Operations Research*, 46(3):946–969, 2021.
- [Fan *et al.*, 2022] Jiaojiao Fan, Isabel Haasler, Johan Karlsson, and Yongxin Chen. On the complexity of the optimal transport problem with graph-structured cost. In *AISTATS*, pages 9147–9165. PMLR, 2022.
- [Goldstein and Osher, 2009] Tom Goldstein and Stanley Osher. The split bregman method for l1-regularized problems. *SIAM journal on imaging sciences*, 2(2):323–343, 2009.
- [Goodfellow *et al.*, 2014] Ian J Goodfellow, Jonathon Shlens, and Christian Szegedy. Explaining and harnessing adversarial examples. *arXiv preprint arXiv:1412.6572*, 2014.
- [Houlsby *et al.*, 2011] Neil Houlsby, Ferenc Huszár, Zoubin Ghahramani, and Máté Lengyel. Bayesian active learning for classification and preference learning. *arXiv preprint arXiv:1112.5745*, 2011.
- [Jacobs *et al.*, 2019] Matt Jacobs, Flavien Léger, Wuchen Li, and Stanley Osher. Solving large-scale optimization problems with a convergence rate independent of grid size. *SIAM Journal on Numerical Analysis*, 57(3):1100–1123, 2019.
- [Ji *et al.*, 2019] Xu Ji, Joao F Henriques, and Andrea Vedaldi. Invariant information clustering for unsupervised image classification and segmentation. In *Proceedings of the IEEE/CVF International Conference on Computer Vision*, pages 9865–9874, 2019.
- [Jia *et al.*, 2022] Xiaojun Jia, Yong Zhang, Baoyuan Wu, Ke Ma, Jue Wang, and Xiaochun Cao. Las-at: Adversarial training with learnable attack strategy. In *CVPR*, pages 13398–13408, 2022.
- [Kannan *et al.*, 2018] Harini Kannan, Alexey Kurakin, and Ian Goodfellow. Adversarial logit pairing. *NIPS*, 2018.
- [Kantorovich, 1942] L Kantorovich. On the transfer of masses (in russian). In *Doklady Akademii Nauk*, volume 37, pages 227–229, 1942.
- [Kurakin *et al.*, 2016] Alexey Kurakin, Ian Goodfellow, and Samy Bengio. Adversarial machine learning at scale. *arXiv preprint arXiv:1611.01236*, 2016.
- [Kwon *et al.*, 2020] Yongchan Kwon, Wonyoung Kim, Joong-Ho Won, and Myunghee Cho Paik. Principled learning method for wasserstein distributionally robust optimization with local perturbations. In *International Conference on Machine Learning*, pages 5567–5576. PMLR, 2020.
- [Lacombe *et al.*, 2021] Julien Lacombe, Julie Digne, Nicolas Courty, and Nicolas Bonneel. Learning to generate wasserstein barycenters. *arXiv preprint arXiv:2102.12178*, 2021.
- [Lee *et al.*, 2020] John Lee, Nicholas P Bertrand, and Christopher J Rozell. Unbalanced optimal transport regularization for imaging problems. *IEEE Transactions on Computational Imaging*, 6:1219–1232, 2020.

- [Li *et al.*, 2018] Wuchen Li, Ernest K Ryu, Stanley Osher, Wotao Yin, and Wilfrid Gangbo. A parallel method for earth mover’s distance. *Journal of Scientific Computing*, 75(1):182–197, 2018.
- [Li *et al.*, 2021] Jincheng Li, Jiezhong Cao, Shuhai Zhang, Yanwu Xu, Jian Chen, and Mingkui Tan. Internal Wasserstein distance for adversarial attack and defense. *arXiv preprint arXiv:2103.07598*, 2021.
- [Madry *et al.*, 2017] Aleksander Madry, Aleksandar Makelov, Ludwig Schmidt, Dimitris Tsipras, and Adrian Vladu. Towards deep learning models resistant to adversarial attacks. *arXiv preprint arXiv:1706.06083*, 2017.
- [Mao *et al.*, 2021] Chengzhi Mao, Mia Chiquier, Hao Wang, Junfeng Yang, and Carl Vondrick. Adversarial attacks are reversible with natural supervision. In *ICCV*, pages 661–671, 2021.
- [Monge, 1781] Gaspard Monge. Memoir on the theory of cuttings and embankments. *Histoire de l’Acad’emie Royale des Sciences de Paris*, 1781.
- [Moosavi-Dezfooli *et al.*, 2016] Seyed-Mohsen Moosavi-Dezfooli, Alhussein Fawzi, and Pascal Frossard. DeepFool: a simple and accurate method to fool deep neural networks. In *CVPR*, pages 2574–2582, 2016.
- [Nie *et al.*, 2022] Weili Nie, Brandon Guo, Yujia Huang, Chaowei Xiao, Arash Vahdat, and Anima Anandkumar. Diffusion models for adversarial purification. *ICML*, 2022.
- [Papernot *et al.*, 2016] Nicolas Papernot, Patrick McDaniel, Somesh Jha, Matt Fredrikson, Z Berkay Celik, and Ananthram Swami. The limitations of deep learning in adversarial settings. In *European symposium on security and privacy*, pages 372–387, 2016.
- [Rebuffi *et al.*, 2021] Sylvestre-Alvise Rebuffi, Sven Gowal, Dan A Calian, Florian Stimberg, Olivia Wiles, and Timothy Mann. Fixing data augmentation to improve adversarial robustness. *arXiv preprint arXiv:2103.01946*, 2021.
- [Scarf, 1957] Herbert E Scarf. *A min-max solution of an inventory problem*. Rand Corporation Santa Monica, 1957.
- [Shi *et al.*, 2021] Changhao Shi, Chester Holtz, and Gal Mishne. Online adversarial purification based on self-supervision. *ICLR*, 2021.
- [Smith and Gal, 2018] Lewis Smith and Yarin Gal. Understanding measures of uncertainty for adversarial example detection. *arXiv preprint arXiv:1803.08533*, 2018.
- [Staib and Jegelka, 2017] Matthew Staib and Stefanie Jegelka. Distributionally robust deep learning as a generalization of adversarial training. In *NIPS workshop on Machine Learning and Computer Security*, volume 3, page 4, 2017.
- [Subramanyam and Raj, 2022] AV Subramanyam and Abhigyan Raj. Barycentric defense. In *ICIP*, pages 2276–2280, 2022.
- [Szegedy *et al.*, 2013] Christian Szegedy, Wojciech Zaremba, Ilya Sutskever, Joan Bruna, Dumitru Erhan, Ian Goodfellow, and Rob Fergus. Intriguing properties of neural networks. *arXiv preprint arXiv:1312.6199*, 2013.
- [Theagarajan *et al.*, 2019] Rajkumar Theagarajan, Ming Chen, Bir Bhanu, and Jing Zhang. Shieldnets: Defending against adversarial attacks using probabilistic adversarial robustness. In *CVPR*, pages 6988–6996, 2019.
- [Wang *et al.*, 2019a] Yisen Wang, Xingjun Ma, James Bailey, Jinfeng Yi, Bowen Zhou, and Quanquan Gu. On the convergence and robustness of adversarial training. In *International Conference on Machine Learning*, 2019.
- [Wang *et al.*, 2019b] Yisen Wang, Difan Zou, Jinfeng Yi, James Bailey, Xingjun Ma, and Quanquan Gu. Improving adversarial robustness requires revisiting misclassified examples. In *International Conference on Learning Representations*, 2019.
- [Wong *et al.*, 2019] Eric Wong, Frank Schmidt, and Zico Kolter. Wasserstein adversarial examples via projected sinkhorn iterations. In *ICML*, pages 6808–6817. PMLR, 2019.
- [Wong *et al.*, 2020] Eric Wong, Leslie Rice, and J Zico Kolter. Fast is better than free: Revisiting adversarial training. *ICLR*, 2020.
- [Wu *et al.*, 2020] Dongxian Wu, Shu-Tao Xia, and Yisen Wang. Adversarial weight perturbation helps robust generalization. *NeurIPS*, 33:2958–2969, 2020.
- [Wu *et al.*, 2021] Boxi Wu, Heng Pan, Li Shen, Jindong Gu, Shuai Zhao, Zhifeng Li, Deng Cai, Xiaofei He, and Wei Liu. Attacking adversarial attacks as a defense. *arXiv preprint arXiv:2106.04938*, 2021.
- [Xie *et al.*, 2019] Cihang Xie, Zhishuai Zhang, Yuyin Zhou, Song Bai, Jianyu Wang, Zhou Ren, and Alan L Yuille. Improving transferability of adversarial examples with input diversity. In *CVPR*, pages 2730–2739, 2019.
- [Xu *et al.*, 2022] Zhuoer Xu, Guanghui Zhu, Changhua Meng, Shiwen Cui, Zhenzhe Ying, Weiqiang Wang, Ming Gu, and Yihua Huang. A2: Efficient automated attacker for boosting adversarial training. *arXiv preprint arXiv:2210.03543*, 2022.
- [Yoon *et al.*, 2021] Jongmin Yoon, Sung Ju Hwang, and Juho Lee. Adversarial purification with score-based generative models. In *ICML*, 2021.
- [Yu *et al.*, 2022] Chaojian Yu, Bo Han, Mingming Gong, Li Shen, Shiming Ge, Bo Du, and Tongliang Liu. Robust weight perturbation for adversarial training. In *IJCAI*, 2022.
- [Zhang *et al.*, 2019] Hongyang Zhang, Yaodong Yu, Jiantao Jiao, Eric Xing, Laurent El Ghaoui, and Michael Jordan. Theoretically principled trade-off between robustness and accuracy. In *ICML*, pages 7472–7482. PMLR, 2019.
- [Zhang *et al.*, 2020] Jingfeng Zhang, Xilie Xu, Bo Han, Gang Niu, Lizhen Cui, Masashi Sugiyama, and Mohan Kankanhalli. Attacks which do not kill training make adversarial learning stronger. In *ICML*, pages 11278–11287. PMLR, 2020.